Failure Behavior for Rocklike Material with Cross Crack under Biaxial Compression

Xuewei Liu[1]; Quansheng Liu[2]; Bin Liu[3]; Yuanguang Zhu[4]; and Penglin Zhang[5]

Abstract: This paper presents an experimental study in which molded gypsum specimens with different crack geometries (T-shaped and X-shaped cross crack) were tested in biaxial compression. Crack propagation and failure behaviors were investigated and nine crack types were detected, namely, wing crack, antiwing crack, secondary crack, horizontal wing crack, quasi-coplanar wing crack, quasi-coplanar secondary crack, far-field crack, surface spalling, and lateral split crack. Moreover, horizontal wing crack and quasi-coplanar wing crack were first observed in the rocklike specimens, which was caused by the added confining pressure. Besides, the cracks and failure modes under uniaxial and biaxial compression were compared according to proposed nine types of new cracks. With an increase in confining pressure, surface spalling and lateral split crack appeared. Lateral split cracks were observed only in T04 ($\sigma_2 = 1.5$ MPa), X03 ($\sigma_2 = 1.0$ MPa), and X04 ($\sigma_2 = 1.5$ MPa), which indicate that lateral split crack is hardly induced under lower confining pressure. The reason is that confining pressure prevents the lateral deformation, therefore, failure can appear only along the free face such as surface spalling and lateral split crack. In practice, surface spalling is the common failure near excavation faces in deep tunnels, which validates the experimental results here. **DOI: 10.1061/(ASCE)MT.1943-5533.0002540.**

Author keywords: Rocklike material; Rock mass; Failure characteristic; Cross crack; Biaxial compression.

Introduction

Understanding the failure behavior of a rock mass with different crack types in biaxial compression is essential for the design and construction of deep tunnels, high rock slope, coal mine roadways, and so on. The stress direction and magnitude around the free face of surrounding rock will change after excavation (Cai and Kaiser 2014). Specifically, the state of the stress on the surface of the rock mass will change from triaxial loading to biaxial loading state, and the magnitude of the stress will increase significantly, which will cause crack propagation and instability of rock mass. The failure mode of rock mass governs the supporting system during the construction. Therefore, it is necessary to study the crack propagation and failure characteristics of rock mass under biaxial compressive stress state.

Crack propagation characteristics of specimens with preexisting cracks have been extensively studied and most of the literature focuses on experimental investigation (Hoek and Bieniawski 1965; Park and Bobet 2009; Wong and Chau 1998; Bobet and Einstein 1998). There are two types of experimental specimens based on their materials. One is real rock specimens, and another one is rocklike specimens. To understand the coalescence behavior, many previous studies have investigated the initiation and propagation process on real jointed rock such as marble (Wong 2008; Cheng et al. 2015), limestone (Feng et al. 2009), granite (Lin et al. 2015; Yin et al. 2014), and sandstone (Lu et al. 2015). Yang and Jing (2011) performed a series of experimental studies to investigate the failure and crack coalescence behavior of brittle sandstone samples under uniaxial compression and identified nine different crack types. The experimental results indicated that the length and angle of fissures have a significant effect on the strength and deformation behavior of sandstone samples. Lee and Jeon (2011) studied crack propagation and coalescence process on granite specimens under uniaxial compression. They found that crack initiation and propagation patterns are affected by material types. Their results indicated that tensile cracks initiated from shear cracks and coalescence occurred mainly through the tensile cracks. Lu et al. (2015) performed a series of uniaxial compression experiments on specimens of sandstone containing a preexisting three-dimensional (3D) surface flaw. Three typical surface cracking patterns were identified and classified by digital photography.

Real rock material can realistically represent the cracking characteristic of engineering rock. However, it is difficult to make multiple artificial cracks in real rock specimens; and it is also hard to get repetitive observations from heterogeneous real rocks. Therefore, the rocklike material plays an important role on studying the cracking process and failure characteristic of rock mass (Zhang et al. 2015; Lee et al. 2017a). The common rocklike materials used in experiments include cement (Cao et al. 2015; Dyskin et al. 2003; Liu et al. 2018), gypsum (Liu et al. 2015; Dyskin et al. 1999; Liu et al. 2016, 2017c), and poly(methyl methacrylate) (PMMA) (Fu et al. 2016). For example, Park and Bobet (2010) experimentally investigated precracked specimens of gypsum material for crack propagation and coalescence from frictional discontinuities. The experiments showed that the crack processes of specimens with

[1]Assistant Professor, State Key Laboratory of Geomechanics and Geotechnical Engineering, Institute of Rock and Soil Mechanics, Chinese Academy of Sciences, Wuhan 430071, China (corresponding author). Email: liuxw@whrsm.ac.cn

[2]Professor, School of Civil Engineering, Key Laboratory of Safety for Geotechnical and Structural Engineering of Hubei Province, Wuhan Univ., Wuhan 430072, China.

[3]Associate Professor, State Key Laboratory of Geomechanics and Geotechnical Engineering, Institute of Rock and Soil Mechanics, Chinese Academy of Sciences, Wuhan 430071, China.

[4]Assistant Professor, State Key Laboratory of Geomechanics and Geotechnical Engineering, Institute of Rock and Soil Mechanics, Chinese Academy of Sciences, Wuhan 430071, China.

[5]Doctor Candidate, School of Civil Engineering, Wuhan Univ., Wuhan 430072, China.

Note. This manuscript was submitted on September 12, 2017; approved on June 15, 2018; published online on November 26, 2018. Discussion period open until April 26, 2019; separate discussions must be submitted for individual papers. This technical note is part of the ***Journal of Materials in Civil Engineering***, © ASCE, ISSN 0899-1561.

open flaws are similar in that with closed flaws. Zhou et al. (2014) investigated the crack initiation, propagation, and coalescence characteristics in cement specimens containing preexisting multiple flaws. The experiment revealed five types of cracks, namely wing cracks, quasi-coplanar secondary cracks, oblique secondary cracks, out-of-plane tensile cracks, and out-of-plane shear cracks. Cao et al. (2015) investigated crack propagation and coalescence of cement specimens with two and three preexisting cracks under uniaxial compression and observed seven types of coalescence. To a certain degree, it is efficient and appropriate to use the rocklike materials to study the complex mechanical behaviors of the natural mass rocks.

Based on the previously mentioned literature, it is indicated that these studies mainly focus on investigating the influence of crack arrangement (including single flaws, two or more flaws) and stress states (under uniaxial and multiaxial compression) on cracking process. Two common characteristics can be concluded: (1) Most of the experiments have used specimens with simple crack geometries (including single crack and multicracks) to study the crack coalescence and failure characteristic. These studies focus on the influence of crack inclination angle, length, width, and crack arrangement on the failure mode. Little literature was reported to study the cracking process of flawed specimen with cross cracks (only Zhang et al. 2012). Therefore, the influence of cross crack on failure behavior needs more research. (2) Most of the previous researches were based on uniaxial compression tests and biaxial compression tests that were occasionally studied. Bobet and Einstein (1998) studied the crack coalescence modes on gypsum specimens with two parallel preexisting cracks under biaxial compression. Their results showed that coalescence and failure occur simultaneously under uniaxial compression but the failure in biaxial compression occurs after coalescence. Yang et al. (2008) investigated strength and failure behavior of precracked marble under conventional triaxial compression and found that crack coalescence mode was closely associated with confining pressure. Sahouryeh et al. (2002) investigated 3D crack growth on specimens with an embedded disklike crack under biaxial compression and indicated that confining pressure changed the crack growth mechanism.

For the biaxial compression tests, only a preexisting crack or two parallel cracks were studied and their results indicated confining pressure can change crack initiation modes but the specific characteristic is not clear. Zhang et al. (2015) indicated that study on specimens only with parallel flaws gives partial understanding of cracking process for natural rock masses because natural rock masses actually have multiple joints in different directions. Therefore, the cracking process and failure characteristics of specimens with cross crack under biaxial compression need further research. In this paper, a series of tests are conducted on specimens with T-shaped and X-shaped cross crack. Crack propagation process and failure behavior for different confining pressures were investigated in detail and influence mechanism of confining pressure on cracking behavior was also studied.

Experimental Details

Specimen Preparation

As shown in Fig. 1, two crack geometries (T-shaped and X-shaped cross crack) were chosen in this test. Both these types of geometry have two preexisting cracks, major and minor crack, respectively. The major crack is inclined at an angle of 45° to the horizontal and two cracks are at a right angle to each other. Both the major and minor cracks are 20-mm long and there is no difference between them. Specifically, σ_1 and σ_2 are the axial loading stress and confining pressure, respectively.

The specimen was produced using gypsum (α-type) with a water–gypsum ratio of 1. The ratio of height and width of specimens was set as 2.0 and the size of the specimen is $60 \times 120 \times 40$ mm and cast in a steel mold. The preexisting cracks were produced with metallic shim. As shown in Fig. 2, the metallic shim is 0.2 mm in thickness, 20 mm in width and 60 mm in length. The metallic shim was inserted into the specimen from the 60×120-mm face and the length and width of the crack is 20 and

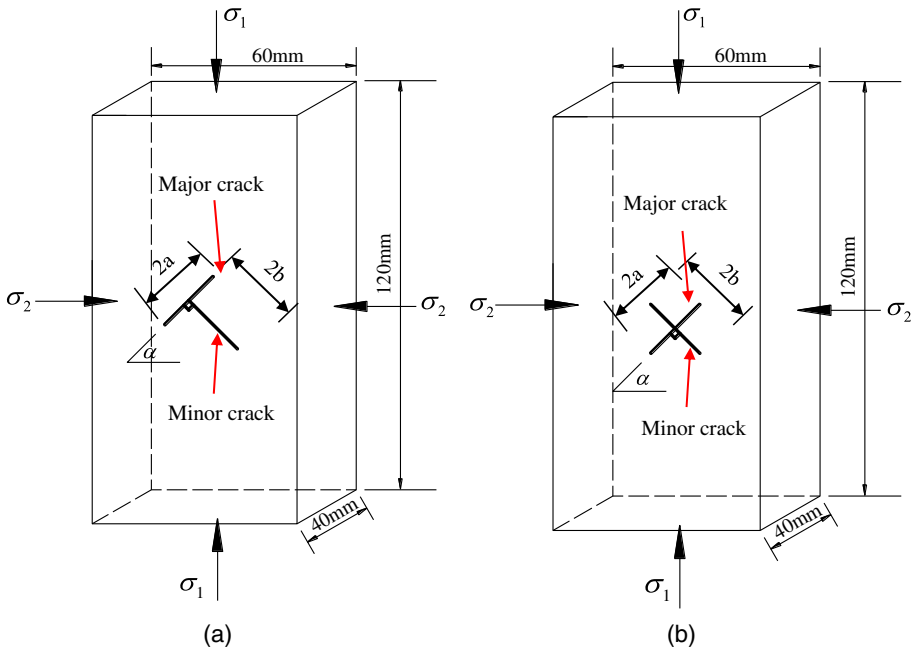

Fig. 1. Specimens with different preexisting crack geometries: (a) T-shaped cross crack specimen; and (b) X-shaped cross crack specimen.

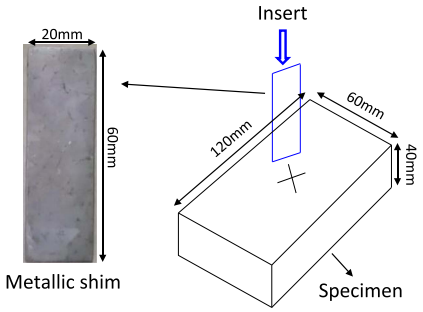

(a)

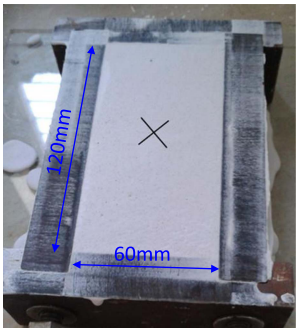

(b)

Fig. 2. Preparation process of preexisting cracks: (a) relationship between metallic shim and cracks; and (b) standard specimen.

0.2 mm, respectively. The preparation process of the specimens can be concluded as follows: (1) weigh and stir the gypsum powder and corresponding water evenly; (2) pour the mixture into the mold and level specimen surface; and (3) produce the cracks and cure the specimens for one month. It is noted that the precracked specimen was used in this paper to represent the specimen with preexisting cracks.

Equipment and Procedure

The tests were conducted using a rock mechanics servo-controlled testing system (RMT-150C manufactured by the Institute of Rock and Soil Mechanics, Chinese Academy of Sciences, China) with the maximum vertical loading capacity of 1 MN. This system can record the data in real time. Additionally, a confining pressure application unit was installed at the loading area of the RMT-150C because it cannot apply the confining pressure. The confining pressure application unit contains oil pump, oil pipeline, pressure stabilizer, and loading equipment. The loading equipment of the confining pressure application unit contains three high stiffness plates and has two spaces, one for the jack to apply pressure and another for mounting the specimens. A high-speed camera (FASTCAM SA5 manufactured by Photron Limited Company, Japan) was used during testing, which can collect, test, and analyze the loading and cracking process of specimens and the frame rate was set as 5,000 fps in this test.

The tests were conducted as follows: Gradually increase the axial and confining pressure with loading rate of 0.4 and 0.2 kN/s until confining pressure reached the designed maximum pressure threshold. Then hold the confining pressure and keep on applying axial pressure with loading rate of 0.02 kN/s until fracture. The designed confining pressures for different specimens are given in Table 1 and tests for specimens with same crack geometry and confining pressure were repeated three times to ensure the test accuracy. It should be noted that the symbols T- and X- given in Table 1 represent a precracked specimen with T-shaped and X-shaped cross crack, respectively.

Table 1. Parameters of different crack types specimens and corresponding confining pressures

Specimen	Confining pressure, σ_2 (MPa)	Description of cracks
Type 1: T-shaped cross crack		Major and minor crack length: 20 mm
T01	0	Angle between the two cracks: 90°
T02	0.5	Major crack inclination angle: 45°
T03	1	
T04	1.5	
Type 2: X-shaped cross crack		
X01	0	
X02	0.5	
X03	1	
X04	1.5	

Results and Discussion

Observations

Fig. 3 shows the typical experimental results of specimens with T-shaped cross crack. From Fig. 3(a), it is clear that for specimen T01($\sigma_2 = 0$ MPa), two new cracks numbered ①$_1$ and ①$_2$ initiated simultaneously from the tips B and D and then propagated along the direction of σ_1. With an increase in loading, two other cracks, ②$_1$ and ②$_2$, initiated from the tip A. Then, a crack numbered ③$_1$ initiated from the tip A and crack ③$_2$ initiated near the tip D along the horizontal directions. Finally, the continuous loading led these six new cracks to propagate forward and to generate a far-field crack ④ during the ultimate failure of the specimen. For specimen T02($\sigma_2 = 0.5$ MPa), it can be found that the cracking process is similar to specimen T01. The difference is that two surface spallings were observed, which were caused by propagation and coalescence of cracks ②$_1$, ②$_2$, and ②$_3$ [Fig. 3(b)]. Except for surface spalling [Fig. 3(c)], a lateral split crack was detected at left side of specimen T04($\sigma_2 = 1.5$ MPa) during the ultimate failure [Fig. 3(d)], which is totally different from the failure mode of specimens T01 and T02.

Fig. 4 shows the typical results of specimens with X-shaped cross crack and Fig. 5 shows axial stress-strain curve of specimen X01. From Figs. 4(a) and 5, the initial axial stress was 3.11 MPa (Point I) for specimen X01($\sigma_2 = 0$ MPa). At this moment, three new cracks numbered ①$_1$, ①$_2$, and ② first initiated from the tips C, D, and near the tip B and then a new crack numbered ③ initiated from the tip C when the axial pressure reached to 3.52 MPa (Point II). Afterward, at the first yielding Point III ($\sigma_1 =$ 3.65 MPa), the cracks ①$_1$ and ② coalesced together and propagated along the direction of σ_1 smoothly. With axial pressure increase to the second yielding Point IV ($\sigma_1 = 3.75$ MPa), other new cracks, ④$_1$, ④$_2$, and ⑤, were initiated and propagated along the direction of σ_1 toward the edge of specimen. Finally, two far-field cracks, ⑥ and ⑦, appeared abruptly near the sides of the specimen and were also observed when the axial pressure reached peak point, V($\sigma_1 =$ 3.91 MPa). For specimens with confining pressure, the test results are similar to the specimens with T-shaped cross crack. By increasing the confining pressure, six surface spalling and four lateral split cracks were observed in specimens X02 and X04, respectively [Figs. 4(b–d)].

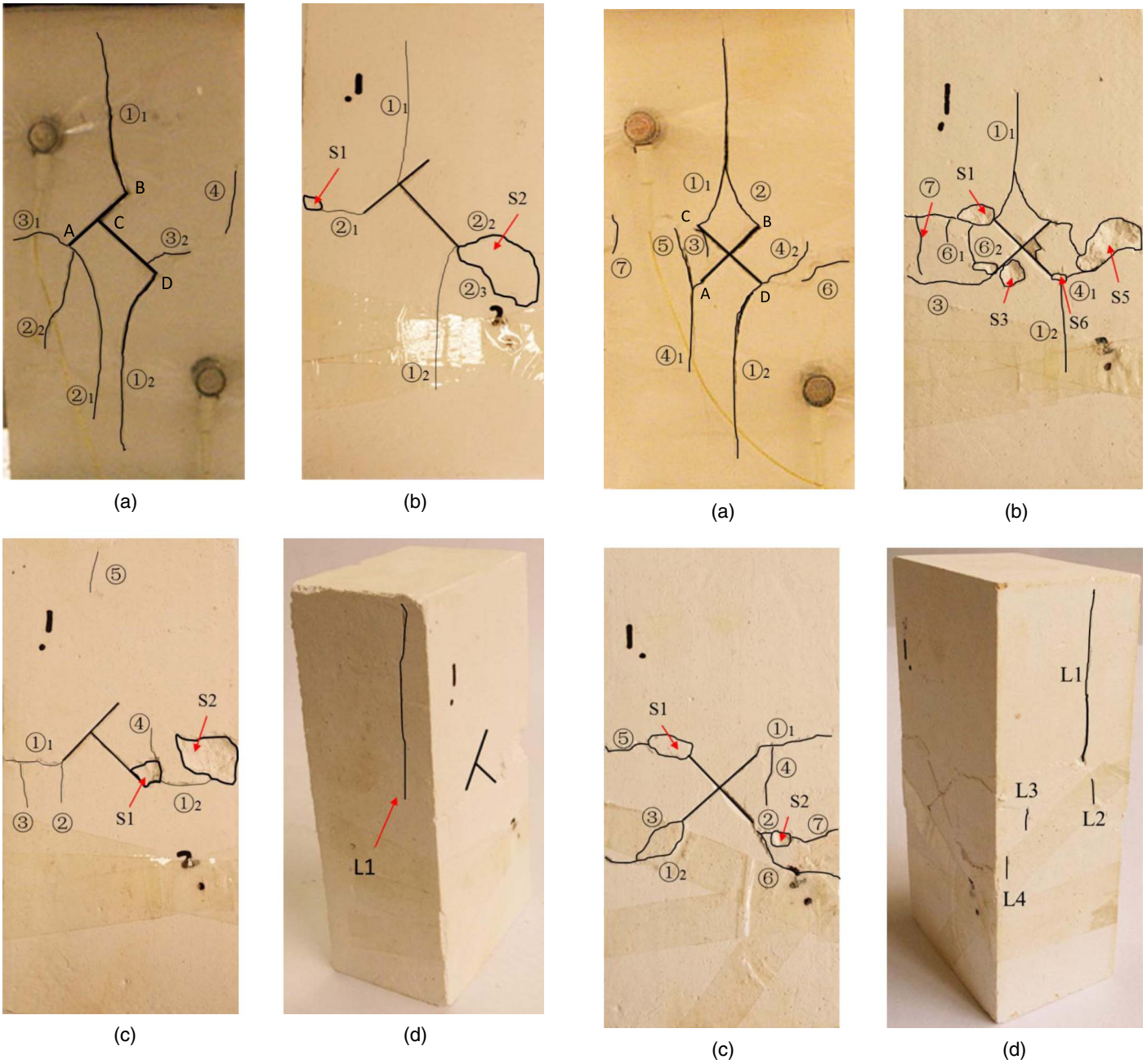

Fig. 3. Failure mode of specimen with T-shaped cross crack: (a) T01 ($\sigma_2 = 0$ MPa); (b) T02 ($\sigma_2 = 0.5$ MPa); (c) T04 ($\sigma_2 = 1.5$ MPa); and (d) T04 (side view of ultimate failure).

Fig. 4. Failure mode of specimen with X-shaped cross crack: (a) X01 ($\sigma_2 = 0$ MPa); (b) X02 ($\sigma_2 = 0.5$ MPa); (c) X04 ($\sigma_2 = 1.5$ MPa); and (d) X04 (side view of ultimate failure).

Discussion

Numerous tests were conducted and two types of crack patterns were observed, namely, wing crack and secondary crack (Shen et al. 1995), as shown in Fig. 6. Wing crack initiates at or near the tips of the preexisting crack and propagates along the direction of principle stress in a stable manner (Park and Bobet 2010; Cao et al. 2015). Some other types of wing cracks such as antiwing crack (Yang and Jing 2011) were also detected. The secondary crack is shear crack and generally occurs after wing crack (Lee et al. 2017b). There are many general secondary cracks such as coplanar secondary crack (Cao et al. 2015), quasi-coplanar secondary crack (Zhou et al. 2014), and oblique secondary crack (Park and Bobet 2009). The shear crack also includes surface spalling because shear crack is rough and covered with powder while tensile crack is smooth and clean (Lajtai 1974).

In this test, nine crack types observed are shown in Fig. 7 and Table 2, which are defined based on the mechanism of initiation and the geometry of the cracks during loading. As shown in Fig. 7, these nine patterns of cracks included wing crack, antiwing crack, secondary crack, horizontal wing crack, quasi-coplanar wing crack, quasi-coplanar secondary crack, far-field or out-of-plane crack, surface spalling, and lateral split crack. Descriptions of these cracks are given in Table 2. Specifically, horizontal wing crack and quasi-coplanar wing crack had not been observed in the rocklike specimens in previous tests. Wong and Einstein (2009) presented an experimental study on molded gypsum specimens

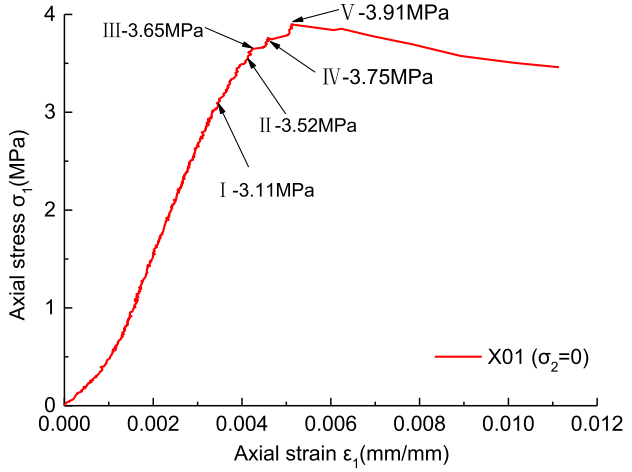

Fig. 5. Several points in axial stress-strain curve of Specimen X01.

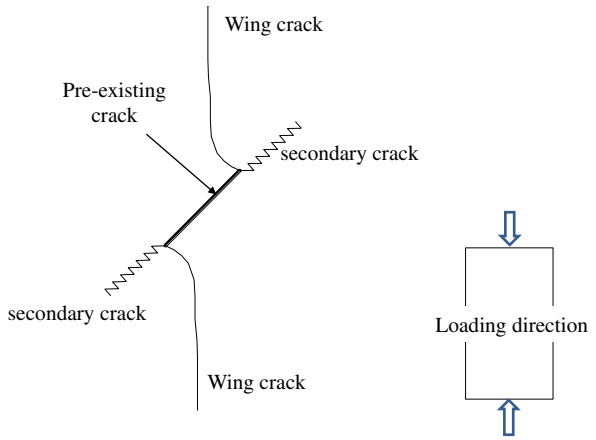

Fig. 6. Crack patterns of jointed specimens in compression. (Adapted from Cao et al. 2015; Shen et al. 1995.)

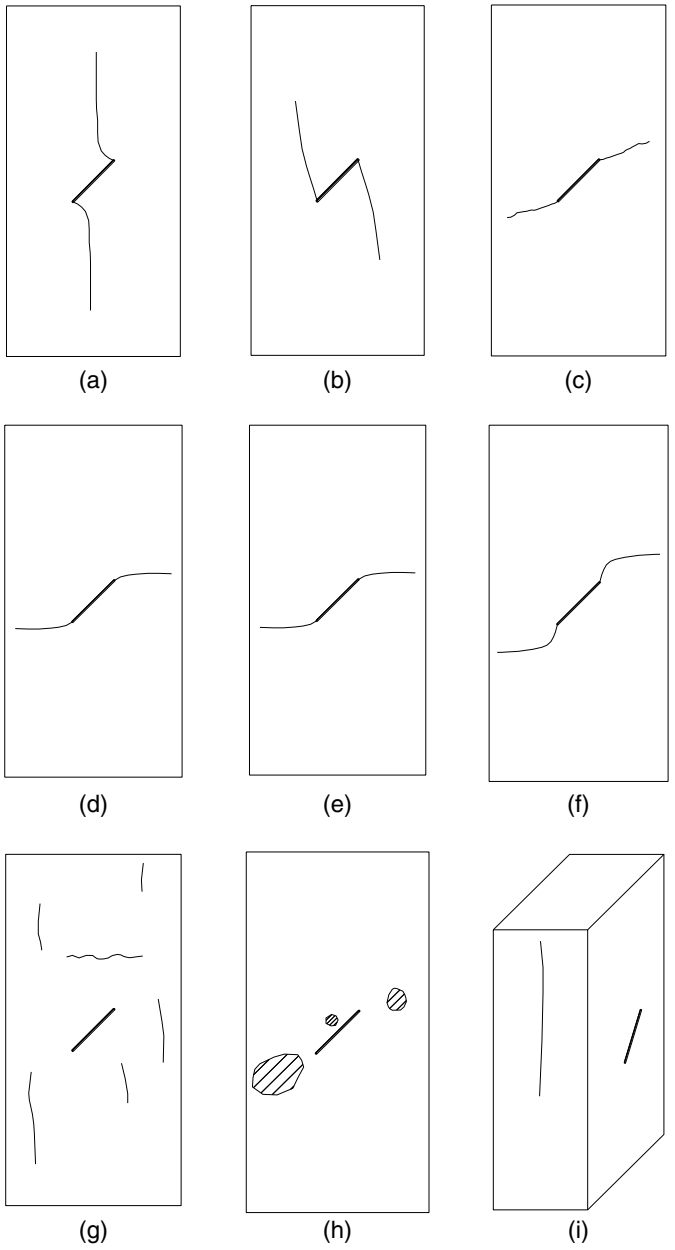

Fig. 7. Crack types observed in tests: (a) Type 1; (b) Type 2; (c) Type 3; (d) Type 4; (e) Type 5; (f) Type 6; (g) Type 7; (h) Type 8; and (i) Type 9.

with a preexisting flaw and indicated that wing crack always initiates along the direction of principle stress. Therefore, the observed horizontal wing crack and quasi-coplanar wing crack are mainly result of confining pressure. In other words, the direction of principle stress was changed by the added confining pressure, which induced the changing of direction of wing crack and hence the new types of wing crack appeared.

Table 3 lists various crack types for all the specimens. As indicated in Table 3, one can conclude that Type 1 wing crack was often observed as the first crack except for the specimens T04 ($\sigma_2 = 1.5$ MPa) and X04 ($\sigma_2 = 1.5$ MPa). For the specimens T04 and X04, horizontal wing crack and quasi-coplanar wing crack were the initial cracks, a pattern different from the other specimens. Lee et al. (2017a) and Cao et al. (2015) indicated that wing crack initiates first and before other cracks, which is in good agreement with the experimental results.

Furthermore, some cracks such as Types 6, 8, and 9 were observed only in specimens under biaxial compression in the present study. Moreover, it is clear that Type 9 (lateral split) cracks were observed only in specimens T04 ($\sigma_2 = 1.5$ MPa), X03 ($\sigma_2 = 1.0$ MPa), and X04 ($\sigma_2 = 1.5$ MPa), which were under higher confining pressure. These results indicated that the lateral split crack was hardly induced in specimens under uniaxial compression or lower confining pressure conditions in present tests. The main reason is that confining pressure prevents the lateral deformation and failure can appear only along the free face and such a failure appeared as surface spalling and lateral split crack. Li et al. (2017) investigated the relationship between spall strength and confining pressure of rocklike materials and found that spall strength decreases as the confining pressure increases. This result indicated that a higher confining pressure can easily cause a surface spalling failure, which is in good agreement with the results herein.

Therefore, the results here indicated that the stress state can control cracking process and ultimate failure mode of rock mass. This finding is expected to provide a meaningful guidance for rock engineering. When confining pressure is lower, crack propagation and coalescence is the main reason of rock failure. However, there is nearly no uniaxial compression condition in practice and confining pressure near excavation face is really high. In that case,

Table 2. Description of different crack types observed in the tests

Crack type	Crack name	Initiation position	Mode	Direction
Type 1	Wing crack	At or near preexisting crack tips	Tension	Quasi-parallel to the direction of σ_1
Type 2	Antiwing crack	At or near preexisting crack tips	Tension	Along the direction of σ_1
Type 3	Secondary crack	At or near preexisting crack tips	Shearing	Not along the direction of σ_1
Type 4	Horizontal wing crack	Preexisting crack tips	Tension	Quasi-parallel confining pressure σ_2
Type 5	Quasi-coplanar wing crack	Preexisting crack tips	Shearing and tension	Quasi-parallel confining pressure σ_2
Type 6	Quasi-coplanar secondary crack	Preexisting crack tips	Shearing	Quasi-parallel preexisting crack
Type 7	Far-field or out-of-plane crack	Intact rock	Shearing or tension	Random
Type 8	Surface spalling crack	Intact rock	Shearing	N/A
Type 9	Lateral split crack	Lateral of specimen	tension	Quasi-parallel to the direction of σ_1

Note: σ_1 and σ_2 are axial loading stress and confining pressure and the directions of σ_1 and σ_2 are vertical and horizontal.

Table 3. Crack types of specimens for different loading modes and geometries

		Crack type								
Loading mode	Specimen	Type 1	Type 2	Type 3	Type 4	Type 5	Type 6	Type 7	Type 8	Type 9
Uniaxial	T01	X[a]	—	X	—	—	—	X	—	—
	X01	X[a]	X	—	—	—	—	X	—	—
Biaxial	T02	X[a]	—	X	—	—	X	—	X	—
	T03	X[a]	—	X	X	—	—	—	X	—
	T04	X	X	—	X[a]	—	—	—	X	X
	X02	X[a]	—	X	X	X	—	—	X	—
	X03	X[a]	X	—	—	X	—	X	X	X
	X04	—	X	—	X	X[a]	X	—	X	X

[a]Indicates that the particular crack was the first to initiate from or near the preexisting cracks.

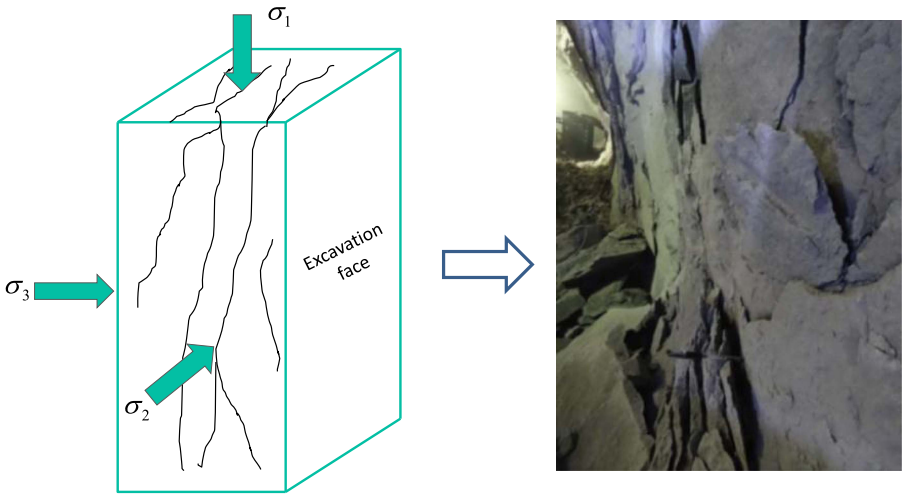

Fig. 8. Stress state and corresponding stress-fracturing in rock mass near underground excavations. (Adapted from Liu et al. 2017a.)

Liu et al. (2017a) indicated that surface spalling and lateral split becomes the typical failure near excavation faces in deep underground engineering (Fig. 8). Therefore, in deep and soft rock tunnel and roadway, steel arch and bolt are generally first used to recover the initial triaxial compression state after excavation, which can prevent the strength of surrounding rock mass decreasing too fast.

Conclusions

The present work determined the failure characteristics of rock mass under biaxial compression based on a series of biaxial compression tests on rocklike precracked specimens with different cracks and confining pressures. Following are the main conclusions:

The crack propagation and failure processes were investigated and nine crack types were observed in the experiments, including wing crack, antiwing crack, secondary crack, horizontal wing crack, quasi-coplanar wing crack, quasi-coplanar secondary crack, far-field crack, surface spalling, and lateral split crack.

Horizontal wing crack and quasi-coplanar wing crack were not found in the rocklike specimens in previous studies. Additionally, horizontal wing crack, quasi-coplanar wing crack, quasi-coplanar secondary crack, surface spalling, and lateral split crack appeared only in the biaxial compressive specimens in this study. Moreover,

lateral split cracks were observed only in T04 ($\sigma_2 = 1.5$ MPa), X03 ($\sigma_2 = 1.0$ MPa), and X04 ($\sigma_2 = 1.5$ MPa), which were under a higher confining pressure. The reason is that confining pressure prevents the lateral deformation; therefore, failure can appear only along the free face.

Finally, it should be noted that this paper investigated some simplified crack geometries under different confining pressure, aimed at obtaining the failure characteristics. The gypsum was used to make precracked specimens as a type of rocklike material. It is known that gypsum is more homogeneous than the real rock and hard to represent the mechanical behavior of real rocks. Rock is heterogeneous solid and gypsum is more homogeneous. Wang and Hu (2017) indicated that crack growth in real rock is more dominated by micrograin structures and gypsum cannot totally describe this phenomenon. In order to deeply understand the characteristics of engineering rock mass under real stress state, more experimental tests for real rocks with different crack parameters under biaxial and even triaxial compression should be conducted in subsequent work.

Acknowledgments

This work was supported by the National Nature Science Foundation of China (Grant Nos. 41602324 and 51774267) and the National Basic Research Program of China (973 Program) (Grant No. 2014CB046904), and China Scholarship Council (No. 201804910219).

References

Bobet, A., and H. H. Einstein. 1998. "Fracture coalescence in rock-type materials under uniaxial and biaxial compression." *Int. J. Rock Mech. Min. Sci.* 35 (7): 863–888. https://doi.org/10.1016/S0148-9062(98)00005-9.

Cai, M., and P. K. Kaiser. 2014. "In-situ rock spalling strength near excavation boundaries." *Rock Mech. Rock Eng.* 47 (2): 659–675. https://doi.org/10.1007/s00603-013-0437-0.

Cao, P., T. Y. Liu, C. Z. Pu, and H. Lin. 2015. "Crack propagation and coalescence of brittle rock-like specimens with pre-existing cracks in compression." *Eng. Geol.* 187: 113–121. https://doi.org/10.1016/j.enggeo.2014.12.010.

Cheng, Y., L. N. Y. Wong, and C. Zou. 2015. "Experimental study on the formation of faults from en-echelon fractures in carrara marble." *Eng. Geol.* 195: 312–326. https://doi.org/10.1016/j.enggeo.2015.06.004.

Dyskin, A. V., L. N. Germanovich, and K. B. Ustinov. 1999. "A 3-D model of wing crack growth and interaction." *Eng. Fract. Mech.* 63 (1): 81–110. https://doi.org/10.1016/S0013-7944(96)00115-4.

Dyskin, A. V., E. Sahouryeh, R. J. Jewell, H. Joer, and K. B. Ustinov. 2003. "Influence of shape and locations of initial 3-D cracks on their growth in uniaxial compression." *Eng. Fract. Mech.* 70 (15): 2115–2136. https://doi.org/10.1016/S0013-7944(02)00240-0.

Feng, X. T., W. Ding, and D. Zhang. 2009. "Multi-crack interaction in limestone subject to stress and flow of chemical solutions." *Int. J. Rock Mech. Min. Sci.* 46 (1): 159–171. https://doi.org/10.1016/j.ijrmms.2008.08.001.

Fu, J. W., K. Chen, W. S. Zhu, X. Z. Zhang, and X. J. Li. 2016. "Progressive failure of new modelling material with a single internal crack under biaxial compression and the 3-D numerical simulation." *Eng. Fract. Mech.* 165: 140–152. https://doi.org/10.1016/j.engfracmech.2016.08.002.

Hoek, E., and Z. T. Bieniawski. 1965. "Brittle fracture propagation in rock under compression." *Int. J. Fract. Mech.* 1 (3): 137–155. https://doi.org/10.1007/BF00186851.

Lajtai, E. J. 1974. "Brittle-fracture in compression." *Int. J. Fract.* 10 (4): 525–536. https://doi.org/10.1007/BF00155255.

Lee, H., and S. Jeon. 2011. "An experimental and numerical study of fracture coalescence in pre-cracked specimens under uniaxial compression." *Int. J. Solids Struct.* 48 (6): 979–999. https://doi.org/10.1016/j.ijsolstr.2010.12.001.

Lee, J., Y. D. Ha, and J. W. Hong. 2017a. "Crack coalescence morphology in rock-like material under compression." *Int. J. Fract.* 203 (1–2): 211–236. https://doi.org/10.1007/s10704-016-0138-2.

Lee, J., J. W. Hong, and J. W. Jung. 2017b. "The mechanism of fracture coalescence in pre-cracked rock-type material with three flaws." *Eng. Geol.* 223: 31–47. https://doi.org/10.1016/j.enggeo.2017.04.014.

Li, X., M. Tao, C. Wu, K. Du, and Q. Wu. 2017. "Spalling strength of rock under different static pre-confining pressures." *Int. J. Impact Eng.* 99: 69–74. https://doi.org/10.1016/j.ijimpeng.2016.10.001.

Lin, P., R. H. C. Wong, and C. A. Tang. 2015. "Experimental study of coalescence mechanisms and failure under uniaxial compression of granite containing multiple holes." *Int. J. Rock Mech. Min. Sci.* 77: 313–327. https://doi.org/10.1016/j.ijrmms.2015.04.017.

Liu, G. F., X. T. Feng, Q. Jiang, Z. Yang, and S. J. Li. 2017a. "In situ observation of spalling process of intact rock mass at large cavern excavation." *Eng. Geol.* 226: 52–69. https://doi.org/10.1016/j.enggeo.2017.05.012.

Liu, Q. S., Q. Liu, Y. Pan, X. W. Liu, X. X. Kong, and P. H. Deng. 2018. "Microcracking mechanism analysis of rock failure in diametral compression tests." *J. Mater. Civ. Eng.* 30 (6): 04018082. https://doi.org/10.1061/(ASCE)MT.1943-5533.0002251.

Liu, Q. S., J. Xu, X. W. Liu, J. Jiang, and B. Liu. 2015. "The role of flaws on crack growth in rock-like material assessed by AE technique." *Int. J. Fract.* 193 (2): 99–115. https://doi.org/10.1007/s10704-015-0021-6.

Liu, X. W., Q. S. Liu, S. B. Huang, L. Wei, and G. F. Lei. 2016. "Fracture propagation characteristic and micromechanism of rock-like specimens under uniaxial and biaxial compression." *Shock Vib.* 2016: 6018291. https://doi.org/10.1155/2016/6018291.

Liu, X. W., Q. S. Liu, L. Wei, and X. Huang. 2017c. "Improved strength criterion and numerical manifold method for fracture initiation and propagation." *Int. J. Geomech.* 17 (5): E4016007. https://doi.org/10.1061/(ASCE)GM.1943-5622.0000676.

Lu, Y., L. Wang, and D. Elsworth. 2015. "Uniaxial strength and failure in sandstone containing a pre-existing 3-D surface flaw." *Int. J. Fract.* 194 (1): 59–79. https://doi.org/10.1007/s10704-015-0032-3.

Park, C. H., and A. Bobet. 2009. "Crack coalescence in specimens with open and closed flaws: A comparison." *Int. J. Rock Mech. Min. Sci.* 46 (5): 819–829. https://doi.org/10.1016/j.ijrmms.2009.02.006.

Park, C. H., and A. Bobet. 2010. "Crack initiation, propagation and coalescence from frictional flaws in uniaxial compression." *Eng. Fract. Mech.* 77 (14): 2727–2748. https://doi.org/10.1016/j.engfracmech.2010.06.027.

Sahouryeh, E., A. V. Dyskin, and L. N. Germanovich. 2002. "Crack growth under biaxial compression." *Eng. Fract. Mech.* 69 (18): 2187–2198. https://doi.org/10.1016/S0013-7944(02)00015-2.

Shen, B., O. Stephansson, H. H. Einstein, and B. Ghahreman. 1995. "Coalescence of fractures under shear stress experiments." *J. Geophys. Res.* 100 (B4): 5975–5990. https://doi.org/10.1029/95JB00040.

Wang, Y., and X. Hu. 2017. "Determination of tensile strength and fracture toughness of granite using notched three-point-bend samples." *Rock Mech. Rock Eng.* 50 (1): 17–28. https://doi.org/10.1007/s00603-016-1098-6.

Wong, L. N. Y. 2008. "Crack coalescence in molded gypsum and carrara marble." Ph.D. thesis, Dept. of Civil and Environmental Engineering, Massachusetts Institute of Technology.

Wong, L. N. Y., and H. H. Einstein. 2009. "Systematic evaluation of cracking behavior in specimens containing single flaws under uniaxial compression." *Int. J. Rock Mech. Min. Sci.* 46 (2): 239–249. https://doi.org/10.1016/j.ijrmms.2008.03.006.

Wong, R. H. C., and K. T. Chau. 1998. "Crack coalescence in a rock-like material containing two cracks." *Int. J. Rock Mech. Min. Sci.* 35 (2): 147–164. https://doi.org/10.1016/S0148-9062(97)00303-3.

Yang, S. Q., Y. Z. Jiang, W. Y. Xu, and X. Q. Chen. 2008. "Experimental investigation on strength and failure behavior of pre-cracked marble under conventional triaxial compression." *Int. J. Solids Struct.* 45 (17): 4796–4819. https://doi.org/10.1016/j.ijsolstr.2008.04.023.

Yang, S. Q., and H. W. Jing. 2011. "Strength failure and crack coalescence behavior of brittle sandstone samples containing a single fissure under

uniaxial compression." *Int. J. Fract.* 168 (2): 227–250. https://doi.org/10.1007/s10704-010-9576-4.

Yin, P., R. H. C. Wong, and K. T. Chau. 2014. "Coalescence of two parallel pre-existing surface cracks in granite." *Int. J. Rock Mech. Min. Sci.* 68: 66–84. https://doi.org/10.1016/j.ijrmms.2014.02.011.

Zhang, B., S. C. Li, X. Y. Yang, D. F. Zhang, C. L. Shao, and W. M. Yang. 2012. "Uniaxial compression tests on mechanical properties of rock mass similar material with cross-cracks." [In Chinese.] *Rock Soil Mech.* 33 (12): 3674–3679.

Zhang, X. P., Q. S. Liu, S. Wu, and X. Tang. 2015. "Crack coalescence between two non-parallel flaws in rock-like material under uniaxial compression." *Eng. Geol.* 199: 74–90. https://doi.org/10.1016/j.enggeo.2015.10.007.

Zhou, X. P., H. Cheng, and Y. F. Feng. 2014. "An experimental study of crack coalescence behaviour in rock-like materials containing multiple flaws under uniaxial compression." *Rock Mech. Rock Eng.* 47 (6): 1961–1986. https://doi.org/10.1007/s00603-013-0511-7.